Superfluid density and critical velocity near the Berezinskii-Kosterlitz-Thouless transition in a two-dimensional strongly interacting Fermi gas

Brendan C. Mulkerin,[1] Lianyi He,[2] Paul Dyke,[1] Chris J. Vale,[1] Xia-Ji Liu,[1,3] and Hui Hu[1]

[1]*Centre for Quantum and Optical Science, Swinburne University of Technology, Melbourne 3122, Australia*

[2]*State Key Laboratory of Low-Dimensional Quantum Physics and Department of Physics, Tsinghua University, Beijing 100084, China*

[3]*Kavli Institute for Theoretical Physics, University of California Santa Barbara, Santa Barbara, California 93106, USA*

(Received 23 February 2017; published 6 November 2017)

We theoretically investigate superfluidity in a strongly interacting Fermi gas confined to two dimensions at finite temperature. Using a Gaussian pair fluctuation theory in the superfluid phase, we calculate the superfluid density and determine the critical temperature and chemical potential at the Berezinskii-Kosterlitz-Thouless transition. We propose that the transition can be unambiguously demonstrated in cold-atom experiments by stirring the superfluid Fermi gas using a red-detuned laser beam, to identify the characteristic jump in the local Landau critical velocity at the superfluid-normal interface, as the laser beam moves across the cloud.

DOI: 10.1103/PhysRevA.96.053608

I. INTRODUCTION

In two-dimensional (2D) many-body systems, topologically nontrivial vortex fluctuations, which are suppressed due to vortex or antivortex binding at low temperature, become amplified above a certain critical temperature, leading to the so-called Berezinskii-Kosterlitz-Thouless (BKT) transition [1–3]. The BKT transition has been of great importance in different branches of physics and has been observed in a range of settings [4–7]. In particular, ultracold atomic gases are an ideal candidate to understand the interaction-driven BKT physics [7], owing to the unprecedented controllability over interatomic interactions, dimensionality, and species [8,9]. Over the past decade, the BKT transition in a 2D weakly interacting Bose gas has been extensively studied by measuring the phase coherence [7,10], confirming the universal equation of state [11,12], probing the superfluidity [13], or observing the free vortex proliferation [7,14,15].

A 2D interacting Fermi gas at the crossover from a Bose-Einstein condensate (BEC) to a Bardeen-Cooper-Schrieffer (BCS) superfluid provides a unique platform to address the *universal* BKT mechanism [16,17], since the underlying character of the system changes from tightly bound composite bosons to loosely bound Cooper pairs of fermions, with decreasing attractions [18]. Indeed, the fermionic BKT transition is now being pursued by several cold-atom laboratories [19–36], and there are indications of the transition from the measurements of pair condensation and correlation function, where (i) the center-of-mass momentum distribution of Cooper pairs, $n_{\mathbf{Q}}$, exhibits anomalous enhancement near $\mathbf{Q} = 0$ below a certain temperature [29] and (ii) the first-order correlation function $g_1(r)$ in real space decays algebraically [30]. However, confirmation of the transition is still to be demonstrated, as these two features may be explained using a strong-coupling theory in the normal phase [37]. This situation marks the importance of having accurate theoretical predictions for the fermionic BKT transition.

The purpose of this research is to apply a strong-coupling theory, beyond the mean field, to a 2D interacting Fermi gas in the *superfluid* phase and present predictions for the BKT critical chemical potential, critical temperature and critical velocity at the whole BEC-BCS crossover. Through a fully *microscopic* calculation of both superfluid density and critical velocity, beyond the phenomenological Landau quasiparticle picture, we predict the occurrence of a significant discontinuity in the critical velocity across the transition as a result of the universal jump in superfluid density [2], which will provide unambiguous proof of the fermionic BKT transition.

The theoretical description of pairing in a 2D interacting Fermi gas at finite temperature is a long-standing challenge due to strongly enhanced quantum and thermal fluctuations. There have been intense theoretical efforts over the past 30 years to understand the corresponding mechanism in 2D layered high-temperature superconductors [18,38,39]. To a large extent, current knowledge of the fermionic BKT transition builds on mean-field approaches [16,17], which break down in two-dimensions as interactions are increased due to fluctuations being larger. There are a number of studies that take into account strong pair fluctuations based on the many-body T-matrix scheme [40–46]; however, these calculations typically focus on the normal state due to technical difficulties. The *ab initio* quantum Monte Carlo (QMC) simulations at finite temperature encounter similar issues [47]. In this work, we consider a Gaussian pair fluctuation (GPF) theory [48–50], which is known to provide a reliable 2D equation of state at zero temperature [44]. We generalize the GPF theory for finite temperatures below the superfluid transition, solving a crucial technical problem of removing divergences in numerics. This enables us to calculate the superfluid density, the key quantity in characterizing the BKT transition, beyond the mean field and taking into account quantum fluctuations. Our main results, as shown in Figs. 3 and 4(b), are of significant importance for further BKT experiments with cold fermions.

The paper is set out as follows, in Sec. II we describe the theoretical model used in calculating the thermodynamic potential and compare the pressure and density equations of state against other theoretical and experimental results where they are available. In Sec. III we calculate the superfluid density and determine the BKT transition to superfluidity. Here we examine the critical chemical for the BKT transition and present a phase diagram of the critical temperature as a function of binding energy. In Sec. IV we consider a

method to unambiguously identify the fermion BKT transition through stirring the cloud with a red-detuned laser. Finally, in Sec. V we consider the conclusion and outlook for future research.

II. THE GPF THEORY AT FINITE TEMPERATURE

A 2D interacting Fermi gas is well described by the Hamiltonian [18]

$$\mathcal{H} = \sum_{\sigma} \bar{\psi}_{\sigma}(\mathbf{r})\mathcal{H}_0\psi_{\sigma}(\mathbf{r}) - U\bar{\psi}_{\uparrow}(\mathbf{r})\bar{\psi}_{\downarrow}(\mathbf{r})\psi_{\downarrow}(\mathbf{r})\psi_{\uparrow}(\mathbf{r}), \quad (1)$$

where $\psi_{\sigma}(\mathbf{r})$ is the annihilation operator for the spin state $\sigma = \uparrow,\downarrow$, $\mathcal{H}_0 = -\hbar^2\nabla^2/(2M) - \mu$ is the kinetic Hamiltonian with atomic mass M, μ is the chemical potential, and U denotes the bare interaction strength of a contact interaction between unlike fermions and is related to the binding energy ε_B via $1/U = \sum_{\mathbf{k}}(\hbar^2\mathbf{k}^2/M + \varepsilon_B)^{-1}$.

Technical details of the GPF theory have been extensively discussed elsewhere [44,48,50]; here, we only present a brief overview of the key equations. Within the GPF framework, we account for strong pair fluctuations at the Gaussian level, beyond the standard mean-field treatment, and consider separately their contributions to the thermodynamic potential $\Omega = \Omega_{\mathrm{MF}} + \Omega_{\mathrm{GF}}$. These two parts can be represented by the BCS Green's function $\mathcal{G}_0(\mathbf{k},i\omega_m)$ and the vertex function $\Gamma(\mathbf{q},i\nu_l)$ (i.e., the Green's function of Cooper pairs): $\Omega_{\mathrm{MF}} = -k_BT\sum_{\mathbf{k},i\omega_m}\ln[-\mathcal{G}_0^{-1}]$ and $\Omega_{\mathrm{GF}} = (k_BT/2)\sum_{\mathbf{q},i\nu_l}\ln[-\Gamma^{-1}]$, that is, the expressions of the thermodynamic potentials for ideal fermions and bosons, where $\omega_m = (2m+1)\pi k_BT$ and $\nu_l = 2\pi l k_BT$ are the fermionic and bosonic Matsubara frequencies with integers m and l, respectively. In other words, the system may be viewed as a *noninteracting* mixture of fermions and pairs. Though the picture is simple, it captures the essential physics for weak and strong interactions. Indeed, at zero temperature, the GPF theory provides a quantitative description of the BEC-BCS crossover in both 3D [48–50] and 2D [44,51]. This can be extended straightforwardly to the general situation where the condensed pairs flow with the wave vector $\mathbf{Q}$, as represented by the pairing gap $\Delta e^{i\mathbf{Q}\cdot\mathbf{r}}$ [52].

In this case, the mean-field thermodynamic potential is given by [52]

$$\Omega_{\mathrm{MF}}(\mathbf{Q}) = \frac{\Delta^2}{U} + \sum_{\mathbf{k}}\left[\tilde{\xi}_{\mathbf{k}} - E_{\mathbf{k}} - \frac{2}{\beta}\ln(1+e^{\beta E^+_{\mathbf{k}}})\right], \quad (2)$$

where $\tilde{\xi}_{\mathbf{k}} \equiv \hbar^2\mathbf{k}^2/(2M) - [\mu - \hbar^2\mathbf{Q}^2/(8M)]$, $E_{\mathbf{k}} \equiv \sqrt{\tilde{\xi}^2_{\mathbf{k}} + \Delta^2}$, $\beta = 1/(k_BT)$, and $E^{\pm}_{\mathbf{k}} \equiv E_{\mathbf{k}} \pm \hbar^2\mathbf{k}\cdot\mathbf{Q}/(2M)$, and to ensure the gapless Goldstone mode, the pairing gap Δ should be calculated using the mean-field gap equation

$$\sum_{\mathbf{k}}\left[\frac{1-2f(E^+_{\mathbf{k}})}{2E_{\mathbf{k}}} - \frac{1}{\hbar^2\mathbf{k}^2/M + \varepsilon_B}\right] = 0, \quad (3)$$

with the Fermi distribution function $f(x) \equiv 1/(e^{\beta x}+1)$. The expression for the thermodynamic potential of pair fluctuations is more subtle [48,50]:

$$\Omega_{\mathrm{GF}}(\mathbf{Q}) = k_BT\sum_{\mathcal{Q}\equiv(\mathbf{q},i\nu_l)}\mathcal{S}(\mathcal{Q})e^{i\nu_l0^+},$$
$$\mathcal{S}(\mathcal{Q}) = \frac{1}{2}\ln\left[1 - \frac{M^2_{12}(\mathcal{Q})}{M_{11}(\mathcal{Q})M_{11}(-\mathcal{Q})}\right] + \ln M_{11}(\mathcal{Q}), \quad (4)$$

where the matrix elements of $-\Gamma^{-1}(\mathcal{Q})$ are given by [52]

$$M_{11}(\mathcal{Q}) = \frac{1}{U} + \sum_{\mathbf{k}}\left[u^2_+u^2_-\frac{1-f^{(+)}_+-f^{(-)}_-}{i\tilde{\nu}_l - E_+ - E_-} - u^2_+v^2_-\frac{f^{(+)}_+-f^{(+)}_-}{i\tilde{\nu}_l - E_+ + E_-} + v^2_+u^2_-\frac{f^{(-)}_+-f^{(-)}_-}{i\tilde{\nu}_l + E_+ - E_-} - v^2_+v^2_-\frac{1-f^{(-)}_+-f^{(+)}_-}{i\tilde{\nu}_l + E_+ + E_-}\right],$$
$$M_{12}(\mathcal{Q}) = \sum_{\mathbf{k}}(u_+v_+u_-v_-)\left[-\frac{1-f^{(+)}_+-f^{(-)}_-}{i\tilde{\nu}_l - E_+ - E_-} - \frac{f^{(+)}_+-f^{(+)}_-}{i\tilde{\nu}_l - E_+ + E_-} + \frac{f^{(-)}_+-f^{(-)}_-}{i\tilde{\nu}_l + E_+ - E_-} + \frac{1-f^{(-)}_+-f^{(+)}_-}{i\tilde{\nu}_l + E_+ + E_-}\right]. \quad (5)$$

Here, we use the short-hand notations $i\tilde{\nu}_l \equiv i\nu_l - \hbar^2\mathbf{q}\cdot\mathbf{Q}/(2M)$, $E_{\pm} \equiv E_{\mathbf{k}\pm\mathbf{q}/2}$, $f^{(\pm)}_{\pm} \equiv f(E^{\pm}_{\mathbf{k}\pm\mathbf{q}/2})$, $u^2_{\pm} = (1 + \tilde{\xi}_{\mathbf{k}\pm\mathbf{q}/2}/E_{\mathbf{k}\pm\mathbf{q}/2})/2$, and $v^2_{\pm} = 1 - u^2_{\pm}$. The density n of the system can be calculated using $n = -\partial(\Omega_{\mathrm{MF}} + \Omega_{\mathrm{GF}})/\partial\mu$, which determines the Fermi wave vector $k_F = (2\pi n)^{1/2}$, the energy $\varepsilon_F = \pi n\hbar^2/M$, and the temperature $T_F = \varepsilon_F/k_B$.

Despite the simplicity and elegance of the GPF theory, it is not easy to solve numerically in general. The technical difficulty comes from the sum over the bosonic Matsubara frequency $i\nu_l$ in Eq. (4), which is divergent. For an interacting 2D Fermi gas at zero temperature the problem may be solved by utilizing an additional function which has no singularities or zeros in the left-hand plane [44,50]. At finite temperature, however, the GPF has only been approximately treated by taking into account the effects of low-energy phonon modes [40,46]. Here, we overcome the divergence by writing [53]

$$\frac{1}{\beta}\sum_{|l|>l_0}\mathcal{S}_{\eta}(\mathbf{q},i\nu_l) = -\frac{1}{\pi}\int_{-\infty}^{+\infty}d\omega\frac{\mathrm{Im}\mathcal{S}_{\eta}(\mathbf{q},\omega+i\gamma)}{e^{\beta\omega}+1}, \quad (6)$$

where $\mathcal{S}_{\eta}(\mathbf{q},i\nu_l) \equiv \mathcal{S}(\mathbf{q},i\nu_l)e^{i\nu_l\eta}$ and $\gamma = (2l_0+1)\pi/\beta$ for the arbitrary positive integer l_0. Thus, the contribution to Ω_{GF} at a given $\mathbf{q}$ can be calculated by using Eq. (6) and taking the remaining discrete sum with $|l| < l_0$, in the limit of $\eta \to 0^+$. We have confirmed that this numerical procedure is robust and independent of the choice of l_0.

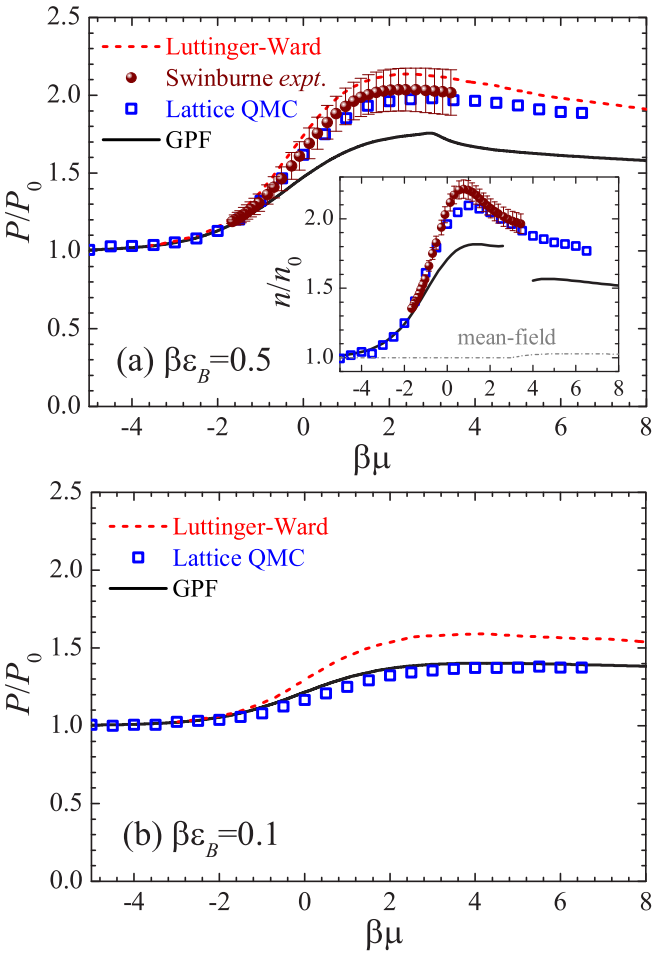

FIG. 1. (a) Pressure equation of state at $\beta\varepsilon_B = 0.5$, where $P = -\Omega/V$. The prediction from the GPF theory (black solid line) is compared with the results from the Luttinger-Ward theory (red dashed line) [42,45], the results from the lattice QMC simulation (blue squares) [47], and the experimental data from Swinburne [33] (solid circles with error bars at a slightly smaller $\beta\varepsilon_B = 0.47$). The inset shows the density equation of state at the same interaction strength. (b) Pressure equation of state at $\beta\varepsilon_B = 0.1$, where the Fermi gas remains normal up to $\beta\mu = 8$. Here, $P_0(\mu)$ and $n_0(\mu)$ are the pressure and the density of an ideal Fermi gas, respectively.

To illustrate the importance of our *full* treatment of the GPF, we show in Fig. 1 the results for the pressure and density equations of state, where $P = -\Omega/V$, at interaction strengths $\beta\varepsilon_B = 0.5$ (a) and $\beta\varepsilon_B = 0.1$ (b) with $\mathbf{Q} = 0$, compared with the predictions from the mean-field theory, above T_c calculations with the self-consistent Luttinger-Ward theory [42,45] and lattice QMC simulation [47], and with recent experimental measurements [33]. It is reasonable from the comparison of results in Fig. 1 that the GPF theory provides a useful description over the whole temperature regime, differing from the lattice QMC and experimental results by ≈10% for the interactions strengths shown. For further comparison of the normal-state calculations of the GPF with experimental results we refer the reader to Ref. [45], where in the normal state the GPF calculations consistently underestimate the density. The discontinuity in the pressure and density equations of state is an unphysical artifact of

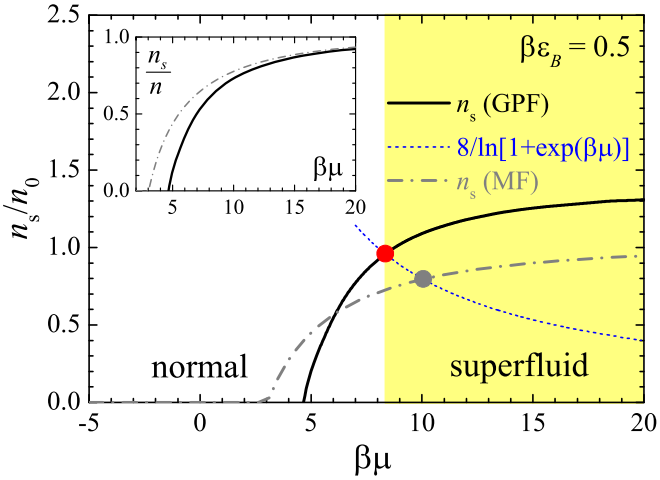

FIG. 2. The superfluid density, in units of the density of an ideal Fermi gas n_0, as a function of the chemical potential at the interaction strength $\beta\varepsilon_B = 0.5$. The GPF and mean-field predictions are shown by the black solid and gray dot-dashed lines, respectively. The circles indicate the critical superfluid density (or chemical potential) for the BKT transition. The inset shows the superfluid fraction n_s/n.

treating the pairing fluctuations at the Gaussian level when calculating the pairing gap Δ and the chemical potential μ; however, the calculation of the superfluid density is still consistent [54]. For a *superfluid* 2D Fermi gas, the GPF theory provides the best description to date, as current mean-field theories strongly underestimate the interaction effects [17] and there are no superfluid QMC calculations at finite temperature. Alternative T-matrix theories have so far focused on the normal state only and predict a 2D superfluid transition at *zero* temperature [38,43]. This is due to the Gaussian fluctuations destroying long-range order at finite temperature in two dimensions.

III. SUPERFLUID DENSITY AND PHASE DIAGRAMS

We now consider the case that the condensed pairs flow with superfluid velocity $\mathbf{v}_s = \hbar\mathbf{Q}/(2M)$. Treating $\mathbf{v}_s$ as small, the superfluid density n_s of the system can be calculated from the lowest-order change in the thermodynamic potential, i.e., $\Delta\Omega = \Omega(\mathbf{v}_s) - \Omega(0) \simeq M n_s \mathbf{v}_s^2/2$, due to the added kinetic energy of the superfluid flow [52], thus, we obtain

$$n_s = \frac{1}{M}\left[\frac{\partial^2\Omega(\mathbf{v}_s)}{\partial v_s^2}\right]_{v_s=0} = \frac{4M}{\hbar^2}\left[\frac{\partial^2\Omega(\mathbf{Q})}{\partial Q^2}\right]_{Q=0}, \quad (7)$$

and the superfluid density can be calculated from the GPF thermodynamic potential of Eq. (4). The BKT critical temperature T_c can then be estimated by self-consistently solving the KT criterion [3,17]:

$$k_B T_c = \frac{\pi}{2}\frac{\hbar^2}{4M} n_s(T_c). \quad (8)$$

Figure 2 reports the GPF superfluid density n_s at the interaction strength $\beta\varepsilon_B = 0.5$, as a function of the dimensionless chemical potential $\beta\mu$. The main figure shows n_s in units of the density of an ideal Fermi gas $n_0 = 2\lambda_T^{-2}\ln(1 + e^{\beta\mu})$, where $\lambda_T \equiv \sqrt{2\pi\hbar^2/(Mk_BT)}$ is the thermal wavelength, while the

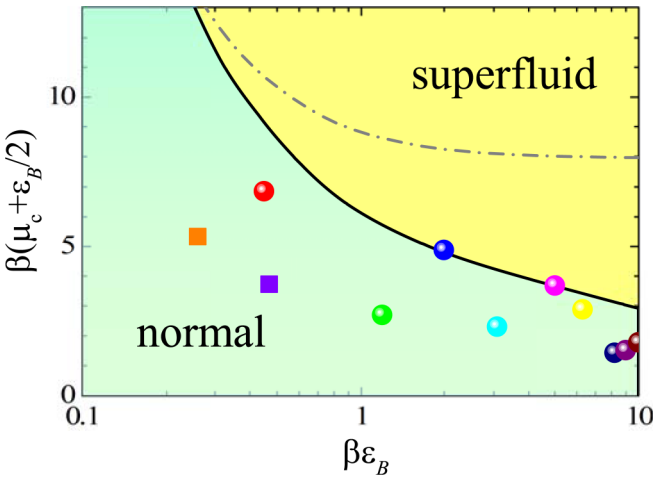

FIG. 3. The critical chemical potential (with $\varepsilon_B/2$ added) as a function of the interaction strength. The black solid line and the gray dot-dashed line show the GPF and mean-field results, respectively. The symbols (in different colors) show the largest chemical potential achieved in the recent density-equation-of-state measurements [33,34], at different interaction strengths.

inset shows the superfluid fraction n_s/n. For comparison, we also plot the mean-field results (dot-dashed lines). By dividing both sides of the KT criterion, Eq. (8), by n_0, we find that the dimensionless critical chemical potential $(\beta\mu)_c$ may be obtained by plotting n_s/n_0 and looking for the intercept with $8/\ln(1+e^{\beta\mu})$. Towards the low-temperature regime, $\beta\mu \to \infty$, the superfluid density calculated using the mean-field theory is typically underestimated, although the superfluid fractions from both mean-field and GPF theories saturate to unity. Consequently, the mean-field theory predicts a larger critical chemical potential.

By repeating the calculations at different interaction strengths we obtain a phase diagram for the critical chemical potential, as shown in Fig. 3. This phase diagram is particularly useful for current cold-atom experiments, where the Fermi gas is confined in a harmonic trapping potential, $V(\mathbf{r})$, and is inhomogeneous. A section of the cloud is locally superfluid if its local chemical potential $\mu_{\rm loc} = \mu - V(\mathbf{r})$ is larger than μ_c. Therefore, experimentally, once the chemical potential at the trap center, μ, and the temperature, T, are measured by fitting the density equation of state at the edge of the cloud with the known virial expansion [33], one can then determine the superfluid radius of the Fermi cloud from our phase diagram, Fig. 3. To make a close connection with experiments, in Fig. 3 we show the largest chemical potential achieved in recent equation-of-state measurements [33,34]. It is encouraging to see that the experiment was approaching the BKT transition.

On the theoretical side, it is of interest to determine the phase diagram for the parameter space of T_c/T_F and $\varepsilon_B/\varepsilon_F$, where we calculate the superfluid fraction as a function of T/T_F. A typical prediction at $\varepsilon_B/\varepsilon_F = 0.1$ is illustrated in Fig. 4(a) by solid circles, contrasted with the mean-field result (dot-dashed line). The superfluid density of a 2D interacting Fermi gas has been recently calculated by Bighin and Salasnich [46] using Landau's phenomenological formulation for the normal density and the quasiparticle spectrum based on the

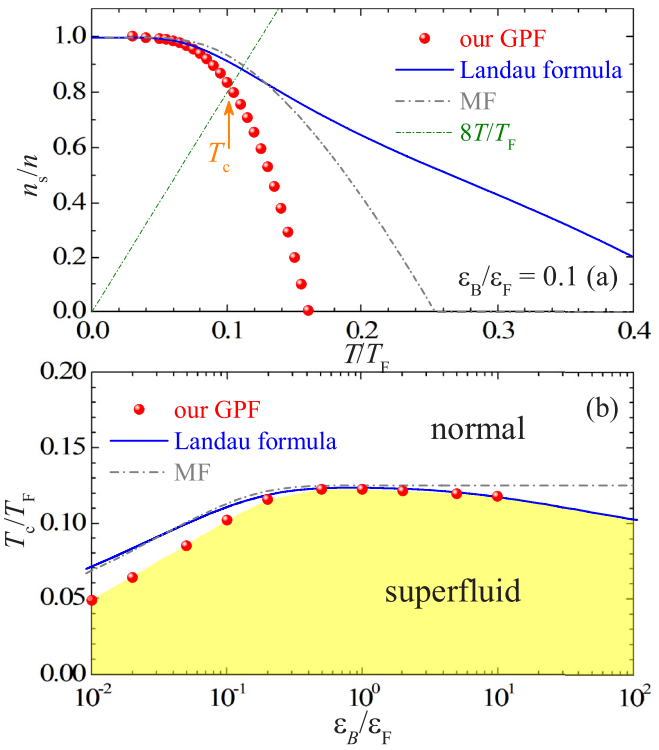

FIG. 4. (a) The superfluid fraction as a function of temperature at interaction strength $\varepsilon_B = 0.1\varepsilon_F$. Our GPF prediction (red circles) is compared with the mean-field result (gray dot-dashed line) and the approximated result based on the zero-temperature GPF (blue solid line) [46]. The intersection with the curve $8T/T_F$ determines the BKT transition temperature. (b) The critical temperature as a function of $\varepsilon_B/\varepsilon_F$.

zero-temperature GPF equation of state [55]. Their result is plotted in Fig. 4(a) for comparison. We find that the prediction of Landau's formulation agrees well with our full GPF calculation at low temperatures, where $n_s/n \sim 1$, but significantly overestimates the superfluid fraction when the temperature becomes larger. According to the KT criterion, the critical temperature T_c/T_F can be extracted by locating the intercept point between the curves n_s/n and $8T/T_F$ and the resulting phase diagram is reported in Fig. 4(b). Our result shows a significant improvement on the BCS side over the previous theoretical predictions [17,46], while on the BEC side (i.e., $\varepsilon_B > 0.5\varepsilon_F$) our result follows closely the approximate prediction from Landau's formula, since in the latter the superfluid fraction at low temperatures $T \sim 0.1T_F$ is reasonably approximated. In the deep BEC regime our GPF result approaches the anticipated BKT critical temperature of a weakly interacting Bose gas [46,56], since the molecular scattering length is correctly reproduced in the GPF theory [44,57]. In this respect, the phase diagram Fig. 4(b) gives a coherent picture across the whole BEC-BCS crossover.

IV. PROBING THE FERMIONIC BKT TRANSITION

We now consider a method to unambiguously identify the fermionic BKT transition. Due to strong interactions, measurements of both phase coherence and free vortex

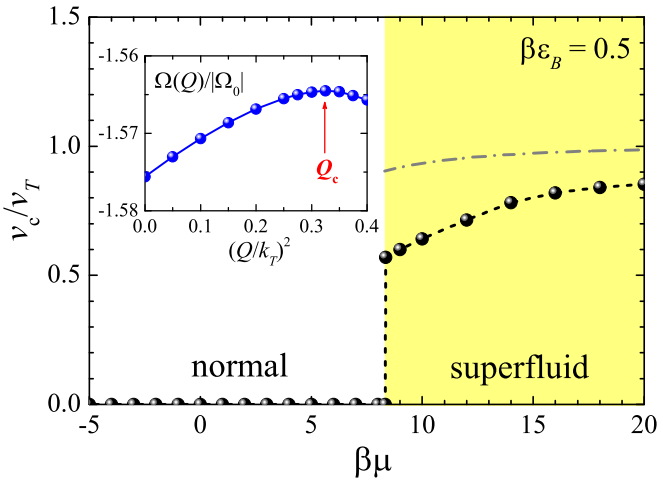

FIG. 5. The critical velocity v_c, in units of the thermal velocity $v_T \equiv [k_B T/(2M)]^{1/2} = \hbar k_T/(2M)$, as a function of $\beta\mu$ at the interaction strength $\beta\varepsilon_B = 0.5$. The black circles (with dashed line) and the gray dot-dashed line show the GPF and mean-field predictions, respectively. The inset shows the thermodynamic potential at nonzero superfluid velocity $v = \hbar Q/(2M)$, which exhibits a local maximum at v_c.

proliferation, which are efficient for a weakly interacting 2D Bose gas, do not work well. Instead, we follow the idea of the superfluidity measurement [13,58,59] and propose to observe the superfluid behavior of an interacting 2D Fermi gas by stirring the cloud with a red- or blue-detuned laser beam. When the Fermi cloud is in the superfluid state, we anticipate that the measured critical velocity will have a sudden jump as the position of the stirred beam moves across the critical radius r_c, which corresponds to the critical chemical potential $\mu_c = \mu - V(r_c)$. This sudden increase is caused by the universal jump in the superfluid density, since *just* below (above) the BKT critical temperature (chemical potential), the finite superfluid density is able to support nonzero superfluid flow [60,61].

Theoretically, we calculate the critical velocity from the velocity dependence of the thermodynamic potential $\Omega(\mathbf{v})$ at a given temperature, T. With increasing superfluid flow, the loss of stability of the system is indicated by the appearance of a local maximum in the thermodynamic potential (see the Appendix for a detailed discussion), as illustrated in the inset of Fig. 5. The determined critical velocity at the interaction strength $\beta\varepsilon_B = 0.5$ is presented in the main figure. The apparent discontinuity at $(\beta\mu)_c \sim 8$ serves as a smoking-gun signature for the BKT transition. To give some realistic numbers, consider a single 2D cloud of $N = 40\,000$ neutral ^{6}Li atoms in a hybrid optical-magnetic trap with frequency $\omega_x \simeq \omega_y \sim 2\pi \times 25$ Hz at temperature $T \sim 20$ nK and at binding energy $\varepsilon_B = 10$ nK (satisfying $\beta\varepsilon_B \sim 0.5$), which is within the regime attainable at Swinburne University of Technology, Melbourne, Australia [33]. The chemical potential at the trap center is estimated to be $\mu \sim 240$ nK. Thus, the superfluid radius is about $r_c \sim 100$ μm, and from Fig. 5, the anticipated jump in the critical velocity would be about $\Delta v_c \simeq 0.6 v_T \sim 4.5$ mm/s, which is readily detectable [58].

V. CONCLUSION AND OUTLOOK

In this paper, we have determined the thermodynamic potential and superfluid density of a two-dimensional Fermi gas at finite temperature for the BEC-BCS crossover, taking into account the strong-coupling pair fluctuation effects at the Gaussian level, beyond previous mean-field calculations. We have overcome the numerical difficulties through a method of summing the Matsubara frequencies, allowing for efficient computation of the superfluid density.

With the calculation of the superfluid density and using the KT criterion we detailed the superfluid transition temperature of a strongly interacting 2D Fermi gas. We find phase diagrams for the critical chemical potential and temperature as a function of interaction strength and predict the occurrence of a significant discontinuity in the critical velocity across the transition as a result of the universal jump in superfluid density. This work provides estimates for the prediction of the fermionic Berezinskii-Kosterlitz-Thouless transition for the whole BEC-BCS crossover, and our results support ongoing cold-atom experiments to unambiguously observe the fermionic BKT transition through the microscopic calculation of both superfluid density and critical velocity. Our approach may also be useful for understanding the superfluid phases of the 2D Hubbard model [62].

ACKNOWLEDGMENTS

We are grateful to Joaquín Drut for sharing the QMC results in Ref. [47] and to Yvan Castin and Gora Shlyapnikov for stimulating discussions on the sudden jump in the critical velocity. This research was supported under Australian Research Council (ARC) Discovery Projects funding scheme (Projects No. DP140100637 and No. DP140103231) and ARC Future Fellowships funding scheme (Projects No. FT130100815 and No. FT140100003). L.H. was supported by the Thousand Young Talents program in China. X.J.L. was supported in part by the National Science Foundation under Grant No. NSF PHY-1125915, during her visit to KITP.

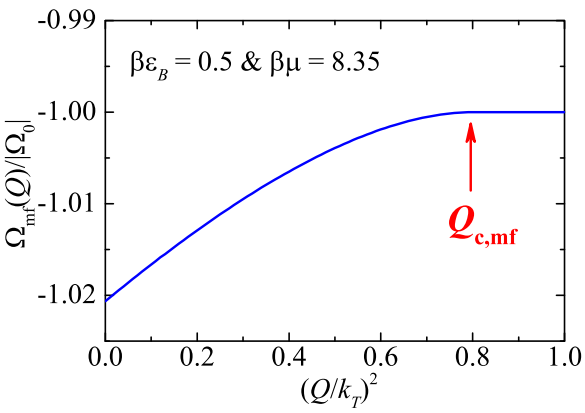

FIG. 6. The mean-field thermodynamic potential at nonzero superfluid velocity $v = \hbar Q/(2M)$, which saturates to the ideal gas thermodynamic potential Ω_0 at the pair-breaking velocity v_{pb}. Here we take $\beta\varepsilon_B = 0.5$ and $\beta\mu = 8.35$.

APPENDIX: VELOCITY DEPENDENCE OF THE MEAN-FIELD THERMODYNAMIC POTENTIAL

In this appendix, we examine the mean-field thermodynamic potential as a function of the superfluid velocity $v = \hbar Q/(2M)$ in the weakly interacting regime with $\beta\varepsilon_B = 0.5$ and $\beta\mu = 8.35$. As shown in Fig. 6, the thermodynamic potential increases with increasing velocity and saturates to its maximum value (which is the ideal gas thermodynamic potential), *precisely* at the pair-breaking velocity [60],

$$v_{\rm pb} = \left[\frac{\sqrt{\mu^2 + \Delta_{mf}^2(Q=0)} - \mu}{M}\right]^{1/2} \simeq 0.9 v_T. \quad \text{(A1)}$$

At this pair-breaking velocity, the pairing gap becomes zero and the system is no longer superfluid [60]. As the system is in the weakly interacting regime (i.e., $\varepsilon_B/\varepsilon_F \sim \varepsilon_B/\mu \sim 0.05$ or $\Delta_{mf}(Q=0)/\mu \sim 0.3$), the sound velocity of the phonon mode $v_s \sim 4v_T$ is larger than $v_{\rm pb}$ and hence the critical velocity of the system is given by $v_{\rm pb}$, according to Landau's picture. Therefore, we observe that within the mean field, the thermodynamic potential attains its maximum at the critical velocity.

By taking into account the strong pair fluctuations beyond the mean field, we anticipate that the thermodynamic potential will exhibit a local maximum as the superfluid velocity increases. This creates an energy barrier. Once the barrier is overcome, the system may lose its superfluidity. The velocity at the local maximum can then be reasonably interpreted as the critical velocity.

[1] V. L. Berezinskii, Sov. Phys. JETP **34**, 610 (1972).
[2] J. M. Kosterlitz and D. J. Thouless, J. Phys. C **6**, 1181 (1973).
[3] D. R. Nelson and J. M. Kosterlitz, Phys. Rev. Lett. **39**, 1201 (1977).
[4] D. J. Bishop and J. D. Reppy, Phys. Rev. Lett. **40**, 1727 (1978).
[5] D. J. Resnick, J. C. Garland, J. T. Boyd, S. Shoemaker, and R. S. Newrock, Phys. Rev. Lett. **47**, 1542 (1981).
[6] A. I. Safonov, S. A. Vasilyev, I. S. Yasnikov, I. I. Lukashevich, and S. Jaakkola, Phys. Rev. Lett. **81**, 4545 (1998).
[7] Z. Hadzibabic, P. Krüger, M. Cheneau, B. Battelier, and J. Dalibard, Nature (London) **441**, 1118 (2006).
[8] I. Bloch, J. Dalibard, and W. Zwerger, Rev. Mod. Phys. **80**, 885 (2008).
[9] R. Onofrio, Phys.-Usp. **59**, 1129 (2016).
[10] P. Cladé, C. Ryu, A. Ramanathan, K. Helmerson, and W. D. Phillips, Phys. Rev. Lett. **102**, 170401 (2009).
[11] C. L. Hung, X. Zhang, N. Gemelke, and C. Chin, Nature (London) **470**, 236 (2011).
[12] T. Yefsah, R. Desbuquois, L. Chomaz, K. J. Günter, and J. Dalibard, Phys. Rev. Lett. **107**, 130401 (2011).
[13] R. Desbuquois, L. Chomaz, T. Yefsah, J. Léonard, J. Beugnon, C. Weitenberg, and J. Dalibard, Nat. Phys. **8**, 645 (2012).
[14] V. Schweikhard, S. Tung, and E. A. Cornell, Phys. Rev. Lett. **99**, 030401 (2007).
[15] J.-y. Choi, S. W. Seo, and Y.-i. Shin, Phys. Rev. Lett. **110**, 175302 (2013).
[16] W. Zhang, G.-D. Lin, and L.-M. Duan, Phys. Rev. A **78**, 043617 (2008).
[17] L. Salasnich, P. A. Marchetti, and F. Toigo, Phys. Rev. A **88**, 053612 (2013).
[18] S. Schmitt-Rink, C. M. Varma, and A. E. Ruckenstein, Phys. Rev. Lett. **63**, 445 (1989).
[19] K. Martiyanov, V. Makhalov, and A. Turlapov, Phys. Rev. Lett. **105**, 030404 (2010).
[20] M. Feld, B. Fröhlich, E. Vogt, M. Koschorreck, and M. Köhl, Nature (London) **480**, 75 (2011).
[21] B. Fröhlich, M. Feld, E. Vogt, M. Koschorreck, W. Zwerger, and M. Köhl, Phys. Rev. Lett. **106**, 105301 (2011).
[22] P. Dyke, E. D. Kuhnle, S. Whitlock, H. Hu, M. Mark, S. Hoinka, M. Lingham, P. Hannaford, and C. J. Vale, Phys. Rev. Lett. **106**, 105304 (2011).
[23] A. A. Orel, P. Dyke, M. Delehaye, C. J. Vale, and H. Hu, New J. Phys. **13**, 113032 (2011).
[24] M. Koschorreck, D. Pertot, E. Vogt, B. Fröhlich, M. Feld, and M. Köhl, Nature (London) **485**, 619 (2012).
[25] A. T. Sommer, L. W. Cheuk, M. J. H. Ku, W. S. Bakr, and M. W. Zwierlein, Phys. Rev. Lett. **108**, 045302 (2012).
[26] Y. Zhang, W. Ong, I. Arakelyan, and J. E. Thomas, Phys. Rev. Lett. **108**, 235302 (2012).
[27] V. Makhalov, K. Martiyanov, and A. Turlapov, Phys. Rev. Lett. **112**, 045301 (2014).
[28] W. Ong, C. Cheng, I. Arakelyan, and J. E. Thomas, Phys. Rev. Lett. **114**, 110403 (2015).
[29] M. G. Ries, A. N. Wenz, G. Zürn, L. Bayha, I. Boettcher, D. Kedar, P. A. Murthy, M. Neidig, T. Lompe, and S. Jochim, Phys. Rev. Lett. **114**, 230401 (2015).
[30] P. A. Murthy, I. Boettcher, L. Bayha, M. Holzmann, D. Kedar, M. Neidig, M. G. Ries, A. N. Wenz, G. Zürn, and S. Jochim, Phys. Rev. Lett. **115**, 010401 (2015).
[31] P. Dyke, K. Fenech, T. Peppler, M. G. Lingham, S. Hoinka, W. Zhang, S.-G. Peng, B. Mulkerin, H. Hu, X.-J. Liu, and C. J. Vale, Phys. Rev. A **93**, 011603(R) (2016).
[32] K. Martiyanov, T. Barmashova, V. Makhalov, and A. Turlapov, Phys. Rev. A **93**, 063622 (2016).
[33] K. Fenech, P. Dyke, T. Peppler, M. G. Lingham, S. Hoinka, H. Hu, and C. J. Vale, Phys. Rev. Lett. **116**, 045302 (2016).
[34] I. Boettcher, L. Bayha, D. Kedar, P. A. Murthy, M. Neidig, M. G. Ries, A. N. Wenz, G. Zurn, S. Jochim, and T. Enss, Phys. Rev. Lett. **116**, 045303 (2016).
[35] C. Cheng, J. Kangara, I. Arakelyan, and J. E. Thomas, Phys. Rev. A **94**, 031606(R) (2016).
[36] For the latest review, see A. V. Turlapov and M. Yu. Kagan, J. Phys.: Condens. Matter **29**, 383004 (2017).
[37] M. Matsumoto, D. Inotani, and Y. Ohashi, Phys. Rev. A **93**, 013619 (2016).
[38] V. M. Loktev, R. M. Quick, and S. G. Sharapov, Phys. Rep. **349**, 1 (2001).
[39] P. A. Lee, N. Nagaosa, and X.-G. Wen, Rev. Mod. Phys. **78**, 17 (2006).
[40] S. N. Klimin, J. Tempere, and J. T. Devreese, New J. Phys. **14**, 103044 (2012).

[41] R. Watanabe, S. Tsuchiya, and Y. Ohashi, Phys. Rev. A **88**, 013637 (2013).
[42] M. Bauer, M. M. Parish, and T. Enss, Phys. Rev. Lett. **112**, 135302 (2014).
[43] F. Marsiglio, P. Pieri, A. Perali, F. Palestini, and G. C. Strinati, Phys. Rev. B **91**, 054509 (2015).
[44] L. He, H. Lü, G. Cao, H. Hu, and X.-J. Liu, Phys. Rev. A **92**, 023620 (2015).
[45] B. C. Mulkerin, K. Fenech, P. Dyke, C. J. Vale, X.-J. Liu, and H. Hu, Phys. Rev. A **92**, 063636 (2015).
[46] G. Bighin and L. Salasnich, Phys. Rev. B **93**, 014519 (2016).
[47] E. R. Anderson and J. E. Drut, Phys. Rev. Lett. **115**, 115301 (2015).
[48] H. Hu, X.-J. Liu, and P. D. Drummond, Europhys. Lett. **74**, 574 (2006).
[49] H. Hu, P. D. Drummond, and X.-J. Liu, Nat. Phys. **3**, 469 (2007).
[50] R. B. Diener, R. Sensarma, and M. Randeria, Phys. Rev. A **77**, 023626 (2008).
[51] H. Shi, S. Chiesa, and S. Zhang, Phys. Rev. A **92**, 033603 (2015).
[52] E. Taylor, A. Griffin, N. Fukushima, and Y. Ohashi, Phys. Rev. A **74**, 063626 (2006).
[53] J. Tempere, S. N. Klimin, J. T. Devreese, and V. V. Moshchalkov, Phys. Rev. B **77**, 134502 (2008).
[54] N. Fukushima, Y. Ohashi, and E. Taylor, and A. Griffin, Phys. Rev. A **75**, 033609 (2007).
[55] G. Baym and C. J. Pethick, Phys. Rev. A **88**, 043631 (2013).
[56] D. S. Petrov, M. A. Baranov, and G. V. Shlyapnikov, Phys. Rev. A **67**, 031601(R) (2003).
[57] L. Salasnich and F. Toigo, Phys. Rev. A **91**, 011604(R) (2015).
[58] W. Weimer, K. Morgener, V. P. Singh, J. Siegl, K. Hueck, N. Luick, L. Mathey, and H. Moritz, Phys. Rev. Lett. **114**, 095301 (2015).
[59] V. P. Singh, C. Weitenberg, J. Dalibard, and L. Mathey, Phys. Rev. A **95**, 043631 (2017).
[60] H. Yamamura and D. Yamamoto, J. Phys. Soc. Jpn. **84**, 044003 (2015)
[61] This is particularly clear on the BEC side, where the critical velocity is given by the sound velocity, according to Landau's picture. The latter remains finite right at the BKT transition.
[62] T. Paiva, R. R. dos Santos, R. T. Scalettar, and P. J. H. Denteneer, Phys. Rev. B **69**, 184501 (2004).